NANO LETTERS

2008
Vol. 8, No. 7
1866-1871

Confinement and Surface Effects in B and P Doping of Silicon Nanowires

C. R. Leao,† A. Fazzio,†,‡ and Antonio J. R. da Silva*,†

Instituto de Física, Universidade de São Paulo, São Paulo, Brazil, and Centro de Ciências Naturais e Humanas, Universidade Federal do ABC, Santo André, Brazil

Received February 11, 2008; Revised Manuscript Received April 24, 2008

ABSTRACT

Several experimental groups have achieved effective n- and p-type doping of silicon nanowires (SiNWs). However, theoretical analyses on ultrathin SiNWs suggest that dopants tend to segregate to their surfaces, where they would combine with defects such as dangling bonds (DB), becoming electronically inactive. Using fully ab initio calculations, we show that the differences in formation energies among surface and core substitutional sites decrease rapidly as the diameters of the wires increase, indicating that the dopants will be uniformly distributed. Moreover, occurrence of the electronically inactive impurity/DB complex rapidly becomes less frequent for NWs of larger diameters. We also show that the high confinement in the ultrathin SiNWs causes the impurity levels to be deeper than in the silicon bulk, but our results indicate that for NWs of diameters larger than approximately 3 nm the impurity levels recover bulk characteristics. Finally, we show that different surfaces will lead to different dopant properties in the gap.

Semiconductor nanowires and, in particular, silicon nanowires (SiNWs) have been considered as one of the most promising alternatives to the traditional Si-based electronic devices.[1,2] Moreover, they have shown great applicability as nanosensors.[3–5] In part, this is due to the great advances in the synthesis techniques, which allow great control of structural features such as diameter, orientation, and surface passivation.[3,6] Furthermore, unlike other one-dimensional nanosystems such as carbon nanotubes, their properties are not overly sensitive to changes in these structural details. However, as in bulk-like technology, doping is paramount, and it is fundamental to have an atomistic understanding of the effects of impurities in such wires.

There have been experimental[7–11]and theoretical[12,13] studies focusing on this issue. From the experimental point of view, the possibility of using P and B to obtain n-type and p-type doped SiNWs, respectively, has been clearly demonstrated even approaching the metallic regime.[7] From the theoretical side, the main conclusions are that (i) surface and subsurface substitutional sites are energetically more favorable than core ones and that (ii) tetra-coordinated impurities yield shallow levels in the band structure. However, a large number of these dopants would present lower coordination on surface sites, where they would become electronically inactive from the point of view of producing carriers in the band edges. Other theoretical analyses focused on how disorder in the distribution of these impurities affects the electronic transport in the wires.[14] These studies were only performed for ultrathin NWs, from 1.0 to 1.6 nm.

In the present work, we show that (1) the impurities surface segregation and the tendency to form a complex with dangling bonds, previously reported, is mostly an effect of extreme confinement, which is rapidly minimized for larger systems; (2) for wires of diameters above 3 nm, impurities will be rather uniformly distributed both within the bulk as well as on different facets of the wires, where they have different electronic properties; and (3) for ultrasmall NWs, the impurity levels, as expected, have deeper character relative to larger ones. However, as the diameter increases, they rapidly tend to become actual shallow levels. All of the simulations were performed with state of the art ab initio total energy calculations, based on the density functional theory (DFT).[15]

We studied three types of SiNWs with B and P impurities on different sites. Two of these NWs are relatively small, with diameters of approximately 11 Å and 12 Å (NW1 and NW2, respectively, in Figure 1). The main difference between these wires is that the first one has the <001> facets in the canted conformation, whereas the second one has the same facet in the symmetric conformation. A third wire, labeled NW3, has the very same types of facets as NW1 but a diameter of about 23 Å, that is, about twice as much as NW1. All of the surfaces of these wires were saturated by hydrogen atoms. The distances between the impurity atoms and their images were 7.84 Å for NW1 and 7.78 Å for NW2 and NW3. These lattice parameters were optimized for undoped wires. In order to assess the influence of dopant

* Corresponding author. E-mail: ajrsilva@if.usp.br.
† Universidade de São Paulo.
‡ Universidade Federal do ABC.

10.1021/nl080403d CCC: $40.75 © 2008 American Chemical Society
Published on Web 06/05/2008

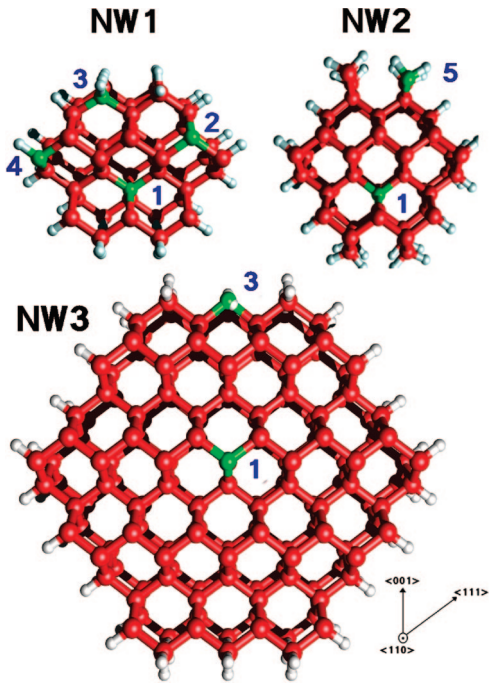

Figure 1. Si nanowires grown along the <110> direction used to study substitutional B and P impurities. NW1 and NW2 possess different types of <001> facets (dihydrated). NW3 has identical types of facets as NW1 but almost twice its diameter. The substitutional sites investigated for each wire are marked in green. Only one impurity per primitive cell was considered.

image proximity in our analyses, we have investigated another wire, which will be labeled NW1-b, that has an identical cross section as NW1, but the distance between the impurity and its image was increased to 19.6 Å. We have also studied boron doping in a Si three-dimentional (3D) crystal, built with 63 Si atoms plus the impurity. The closest distance between dopants and their images in this bulk was 11.0 Å.

Boron and phosphorus dopants in these NWs were always in substitutional sites, indicated in Figure 1. On the surfaces, we studied situations in which the impurities were saturated by two hydrogens (<001> surfaces only) or one hydrogen. The effect of dangling bonds (DBs) was also investigated, considering configurations with no hydrogen at all. We calculated the formation energies, E_f, for all of these sites using the following expression

$$E_f = E_d - E_p + \mu_{Si} - \mu_I + n * \mu_H \quad (1)$$

where E_d (E_p) is the total energy of the doped (undoped) system, μ_{Si} (μ_H) is the chemical potential for the Si (H) atom, μ_I is the chemical potential of the dopant (either B or P), and n is the number of removed H atoms when studying DBs. As we only report relative formation energies, the silicon and the impurities chemical potentials μ_I do not need to be considered. The chemical potential of hydrogen was extracted from the H_2 molecule.

The results for B doping are summarized in Table 1. We note that our results are in disagreement with ref 13, where the position labeled 2 in Figure was found to be the most favorable one for fully passivated SiNWs. As can be seen, the position 3 is the most stable one for fully passivated

Table 1. Relative Formation Energies (Electronvolts), with Respect to the Global Lowest Value (Site 3 with a DB), of a Substitutional B Impurity on Different Sites (see Figure 1), with and without Surface Dangling Bonds (DB)

location	wire	fully passivated	with a DB	with two DB
1	NW1	0.64	0.82/1.38[a]	
	NW2	0.39		
	NW3	0.27		
2	NW1	0.47	0.65[b]	
3	NW1	0.34	0.0	1.80
	NW3	0.21	0.02	
4	NW1	0.51	0.55	
5	NW2	0.42	0.45	2.18

[a] The first (second) value refers to a situation where the DB is present on the <001> (<111>) surface. [b] The DB is on the <111> facet.

wires, and the same position, when boron forms a complex with a dangling bond (B + DB complex), is the most stable site among all considered. In ref 12 and ref 13, the B + DB complex was reported as the most stable position as well; however, these authors seem to have considered this complex only on the <111> surface. We find that for wires of approximately 1 nm diameter this site has higher energy than the B+DB complex on the <100> site, by 0.55 eV. We note that among all surface positions investigated, only on site 3 (NW1 and NW3) the B + DB complex resulted energetically more favorable than the tetracoordinated conformation (i.e., without the DB). In order to rationalize these results, we have performed calculations where a DB was created on these surface sites without allowing the atoms to relax. This gives a measure of the binding energy of the H atoms to the B impurities separated from the atomic relaxation contribution to total energy. We have found that for position 5 in NW2 and position 4 in NW1 these binding energies are 0.7 and 0.6 eV, respectively, whereas for position 3 in NW1 a much lower binding energy of 0.2 eV was found. After letting the system relax, the overall gain due to the atomic relaxation is similar in all cases, being approximately between 0.6 and 0.7 eV. The reason why the binding energy of H on positions 4 and 5 differs so much from that on position 3 is that the hydrogens are canted in the latter one, which is caused by the need to accommodate the electrostatic repulsion at the expense of causing stress in the hydrogen−surface bonds network. This is consistent with the observation that these canted surfaces would be unstable when compared to the symmetric one.[21]

The energy difference between the B atom in the center (without any DB present) of the wire and the B + DB complex in position 3 is 0.64 eV. For the larger NW3 this same energy difference decreases to 0.25 eV. If this trend continues for larger diameters, for wires with $d = 3$ nm or more, these two sites will have similar populations. Moreover, the formation energy of the B impurity on surface site 3 in the fully passivated case and in association with the dangling bond in NW3 decreased in comparison to NW1 by about 44% (0.34 to 0.19 eV). In addition to the evident effects that enlarging the wires' dimensions has in these formation energies, we should remember that the species we used to evaluate the chemical potential of the H atom, the H_2 molecule, yields a fairly high value for this energy

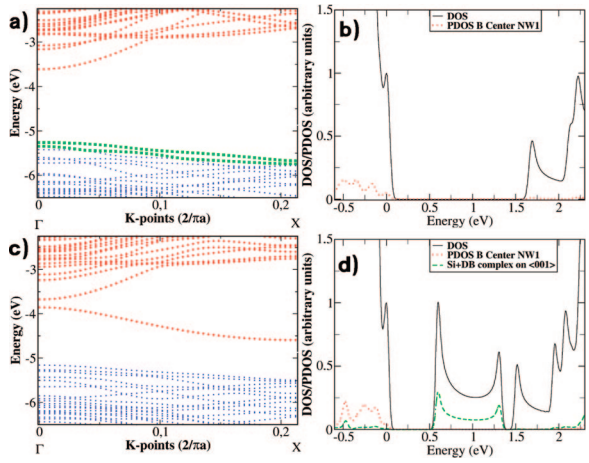

Figure 2. Kohn−Sham band structures of NW1 with a B impurity located at position 1 (Figure 1). (a) No dangling bons are present. (c) There is one DB on the <001> facet. Occupied levels are indicated by blue circles, the empty ones are indicated by red rhombuses and green squares represent semifilled ones. (b,d) We show the corresponding DOS images (black solid lines) and the PDOS on the impurity atom (red dotted line). The dashed green line in d is the PDOS on the Si where the DB is present.

reference. There are other sources of hydrogen atoms during the growth process of the wires, and some of them might yield smaller values for μ_H, resulting that the differences in the formation energy of tetra-coordinated boron dopants and that of the B + DB complexes will be even smaller. In fact, considering that the growth of these wires is performed at high temperatures (between 400−500 °C and in some cases, even up to 1200 °C),[9,10] there will be significant occupation of all sites, both in the bulk as well as on the surfaces. Finally, as the surface to bulk ratio diminishes with increasing diameter, bulk sites will become even more relevant.

Another important finding, at least for ultrasmall wires, is the fact that the formation energy of a dangling bond is strongly reduced in the presence of a B atom even if it is in the center of the NW. We have calculated for an undoped NW the formation energy of a DB, and we found 1.13 eV for the <100> surface. If there was no interaction between the B in the center of the wire and the DB, the formation energy for this configuration would be 0.64 + 1.13 = 1.77 eV. However, we have found a formation energy for a DB on the <100> surface of NW1 with a centrally located boron impurity of 0.82 eV; that is, a decrease of almost 1 eV relative to the isolated formation energies of both defects. This is a result of a charge transfer from the DB to the B acceptor level. In Figure 2, this effect is demonstrated: the B impurity in the center of the fully passivated wire generates semifilled Kohn−Sham levels close to the top of the valence band (indicated by green squares). When a DB on the surface is present, no semifilled states are observed. Levels associated with the impurity get completely filled and there appears an empty level across the band gap of the wire with a strong character of the Si where the DB is present. Thus the presence of DBs in NWs is detrimental to B doping, since they are compensating defects.[12] Finally, we note that the formation energy for the analogous site labeled 1 (Figure 1) in NW2 decreased 0.25 eV relative to NW1, that is, a

Table 2. Relative Formation Energies (Electronvolts), with Respect to the Global Lowest Value (Site 3 with a DB), of a Substitutional P Impurity on Different Sites (See Figure 1), with and without Surface Dangling Bonds (DB)

location	wire	fully passivated	with a D.B.	with two D.B.
1	NW1	1.06		
	NW3	0.79		
3	NW1	1.31	0.0	0.89
	NW3	1.17	0.09	
4	NW1	1.04	0.15	
5	NW2	1.25	0.22	1.28

decrease of almost 40% due to variations on the type of surface. Such changes of the atomic conformation on the surfaces of nanowires imply changes in electronic and structural properties, such as the lattice parameter, which affect the wire as a whole and not only locally on the surfaces.[22] Experimentally, it is possible to identify the conformation of surface atoms. For example, it has been observed[21] that Si NWs present the symmetric conformation for the <001> facet, as in our NW2. As we predict that different surface conformations will lead to distinct most stable positions for dopant atoms in ultrasmall NWs, this indicates that by imaging the atomic surface it may be possible to infer the distribution of dopant atoms in the NWs. For example, in the above-mentioned case of experimentally observed symmetric conformation for the <001> facet, it would be expected that the B atoms would tend to be centrally located.

In Table 2, we summarize the results for P doping. We find that there is a stronger preference to form complexes of P + DB for the ultrathin wires in this case than when they are doped with boron. The surface with the most stable site for tetra-coordinated P impurity is the <111>. However, the other surfaces have formation energies that are relatively similar, and in the presence of the DB, position 3 on <001> facet becomes slightly more favorable than all others. Increasing the wire's diameter, the difference in formation energy between passivated and the unpassivated surface site 3 decreased from 1.31 eV in NW1 to 1.08 eV in NW3, about 18%, which is quite less than in the case of B doping, as discussed above. The formation energy of the centrally located P impurity in NW3 decreased by about 0.37 eV relative to NW1. As a result, the energy difference between the P + DB complex in position 3 and the tetra-coordinated phosphorus in the center of the wire decreased from 1.06 to 0.70 eV; a reduction of nearly 34%. Even though this energy difference is still higher than in the case for the B dopant, it indicates the same trend: as the wires become larger, both types of impurities rapidly get more uniformly distributed within the available sites and the occurrence of the complexes with DB is less frequent.

In the case of doped Si nanocrystals (Si NCs), it has been reported that for larger systems boron impurities tend to be more stable near the surface whereas phosphorus defects present lower formation energy in inner sites.[23–25] Moreover, in the case of P doped Si NCs, it has been shown that for small wires there is a transition where centrally located impurities and surface ones are almost equally probable[25]

(these studies did not consider configurations with a DB). This is what we observe in Table 2 if we consider only tetra-coordinated impurities in NW1 and NW3. At least three effects concur to determine these formation energies: (I) the size of silicon atoms is much closer to phosphorus' than boron's. Therefore, the latter will induce more structural distortions in the Si host than the former. Closer to the surfaces, such distortions can be more easily accommodated. (II) Boron can present either the sp^2 or the sp^3 hybridization depending on whether it is tri- or tetra-coordinated, respectively. Phosphorus always tends to be in an sp^3 configuration, even when it is tricoordinated in association with a surface DB, with a lone pair pointing outward. (III) On the surfaces, the defect state gets more distorted because of the asymmetries in the environment where it is embedded.[25] For smaller systems, however, the energy gain due to this higher local symmetry in the center of the structure is less significant. Combined, these three effects rationalize the data in Tables 1 and 2: surface sites present fairly lower formation energies than bulk sites for B impurities due to effect I), but this is balanced out by point III). Surface or inner tetra-coordinated sites for P dopants do not show such great variations of formation energy due to I but the presence of the dangling bond remains energetically more favorable because of II. As the diameters of the system grow, effect III sets in, resulting that surfaces with a dangling bond is no longer much more favorable than bulk substitutional sites. Therefore, the conclusion of ref 12 that the B + DB complex dominates the doping is only valid for ultrasmall NWs, and we predict a relatively uniform B and P distribution over larger wires.

Both boron and phosphorus are known to be shallow impurities in bulk silicon. This means that these dopants are easily ionized in such a way that it is facile to thermally create free carriers at the band edges. Indeed, we have observed such impurity levels in the Kohn−Sham band structure near the valence band maximum and the conduction band minimum for B (Figure 2a) and P doped wires, respectively, when the impurities were on tetragonal conformation. However, as DFT is designed to optimize the total energy of the system rather than the quasi-particle spectra, instead of simply looking at the position of the Kohn−Sham eigenvalues, a more precise way to determine the position of the impurity state in relation to the band edges is to calculate the crossing between the formation energy curves for the different charge states, $\varepsilon(-/0)$ and $\varepsilon(0/+)$, as a function of electronic chemical potential.[27] We show these charge states crossings in Table 3 together with the Mott-Hubbard energy, U, which is defined as the difference between the affinity and ionization energies. For such purpose, we consider the doped SiNW in three different charge states: neutral (0), with an extra electron (−), and with a missing electron (+), always allowing the system to fully relax. For these calculations, we have used the following expressions:

$$U = E^{+} + E^{-} - 2E^{0} \tag{2}$$

$$\varepsilon(q/0) = E^{q} - E^{0} + q * \varepsilon_{x} \tag{3}$$

where E^q is the total energy of the charge states q (either +1 or −1) and ε_x can be the energy of either the top of the valence band (for $q = -1$) or the bottom of the conduction band (for $q = +1$) of the undoped wire.

In Table 3, we report the U, the $\varepsilon(-/0)$ (B-doped), and the $\varepsilon(0/+)$ (P-doped) for different situations in NW1, NW2, and NW3. As in the wires the impurity and its images are separated by about only 8 Å, it is important to estimate how much this unrealistic proximity among dopants could be affecting the results in Table 3. We thus performed calculations for the B in the center of NW1-b, which has a much larger supercell length along its axis, of 19.6 Å. The U dropped from 1.2 eV in NW1 to 0.45 eV in NW1-b, a reduction of approximately 2.5 times. The ionization level dropped as well, from 0.55 to 0.2 eV.

As such small NWs are still too hard to grow in actual experiments, it is thus important to see how quickly the levels change as a function of diameter. From Table 3, we see that the value of U for B at the center of NW3 is 0.8 eV, about 1.5 times lower than in the center of NW1. If we assume that the effect of increasing the separation between the B atom and its images in the NW3 would be similar to what was observed from NW1 to NW1-b, the U would eventually become of the order of 0.3 eV for a spacing between the impurity and its image of about 19 Å. Comparison of these values with the doped silicon bulk could indicate the depth of the impurity levels. However, dealing with charged systems using methods that employ periodic boundary conditions (PBC) is extremely tricky, as largely discussed in the literature.[28,29] Even though the use of a compensating background potential does prevent the total charge of the system to diverge, the screening provided by this delocalized jellium potential to the extra charge localized at the defect site might not be enough to prevent the spurious electrostatic interaction among supercells. In systems such as nanowires, the subject is even more sensitive because of the presence of a vacuum layer in the supercells. Although enlarging the vacuum layer certainly dumps the unphysical electrostatic interaction among supercells, it does also worsen the screening provided by the jellium, which gets more delocalized with a larger vacuum layer. In the results presented

Table 3. U and Ionization Levels for SiNWs Doped with Boron and Phosphorus on Different Sites[a]

	U (eV)		ε (eV)	
impurity location	B	P	B	P
NW1−1	1.2	1.5	0.55	0.6
NW1b-1	0.45		0.2	
NW2−1	1.25		0.4	
NW1−3	0.6	0.03	0.5	0.4
NW1−4	1.2	1.5	0.55	0.6
NW2−1	1.25		0.4	
NW2−5	1.05	1.5	0.25	0.65
NW3−1	0.8		0.4	
NW3−3	0.75		0.25	
bulk 64[26]	0.30		≈0.0	

[a] A similar analysis for bulk silicon was also performed. ε stands for $\varepsilon(-/0)$ for B doping and $\varepsilon(0/+)$ for P doping.

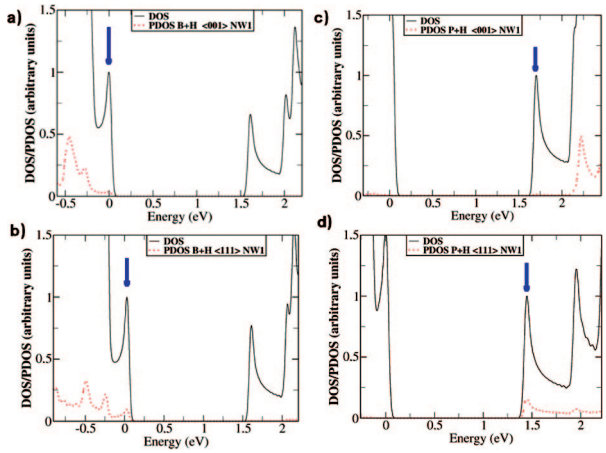

Figure 3. Total density of states (solid black line) and projected DOS on the impurity atoms (dashed red line) on different surface sites of NW1: (a,c) B and P atoms, respectively, in position 3; (b,d) B and P atoms, respectively, in position 4. In all cases, the impurities were tetra-coordinated. The energy zero was set to the first DOS peak at the left of the band gap in all cases, and the DOS curves were normalized by the impurity peak (blue arrows).

in Table 3, we have made several tests in order to set the vacuum layer to achieve the best possible compromise between these two opposing effects.[30] Although previous works have tried to assign a universal nature to the crossing of the charged states in NWs,[31] due to the reasons discussed above comparison between $\varepsilon(q/0)$ in different states should be looked upon with extreme care, and here we present them for relative comparisons.

A simple way to check the accuracy of the results presented in Table 3 is to compare the relative weight of the states associated to the dopant (PDOS) against the total density of states (DOS) of the system at the impurity levels. In Figure 3, we present some PDOS graphs for the NW1 with a boron dopant in positions 3 and 4, (Figure 3a,b, respectively) and similar images for P impurities (Figure 3c,d). The dopant was always tetra-coordinated, without any surface DB in these situations. From these graphs, we notice that the first visible peaks of the PDOS graphs (red dotted lines) associated with the impurities on the canted <001> surface of NW1 are significantly less pronounced relative to the total DOS peak within the gap of the pristine NW, indicated by blue vertical arrows (Figure 3a,c). These DOS peaks are in fact the ones related to the donor/acceptor levels. For the monohydrated <111> facet (Figure 3b,d), these PDOS peaks are much larger relative to the DOS. These differences in the PDOS of the impurities depending on the type of facet in which they are embedded can be understood in terms of how these surface states contribute to the formation of the band edges of the wires. In ref 22, we showed that surfaces whose atoms make bonds to the inner ones only along directions perpendicular to the wires' axes do not contribute significantly to the formation of the band edge states.[22] This is the case of the canted <001> facet in NW1. Therefore, the weight of the dopant atom located on such facet on the impurity state is not very high. On the other hand, the monohydrated <111> surfaces are very active for the formation of the band edge states, implying

Table 4. Ratios between the Projected Density of States of B and P Impurities and the Total Density of States in SiNWs NW1, NW1-b, and NW3[a].

		PDOS/DOS(%)	
impurity location	system	B	P
1	NW1	4.8	8.6
	NW2	4.2	
	NW1-b	2.2	
	NW3	3.3	7.8
3	NW1	3.4	1.1
	NW3	1.3	1.7
4	NW1	9.4	16.0
5	NW2	9.9	20.6
	bulk	1.4	1.5

[a] The ratios were taken at the energy of the impurity induced peak level of the total DOS within the gap of the undoped wires (see Figure 3).

that dopants located on them have a stronger weight at impurity states of the doped wires.

The correlation between the PDOS/DOS ratio and the position of the impurity state relative to the band edges can be better understood if we approximate the problem by a simple two-level model. Let us consider the particular case of B doping, and let us call $|\phi_B\rangle$ the isolated dopant state and $|\psi_{VBE}\rangle$ the valence band edge of the pristine wire, with unperturbed eigenvalues δ_B and δ_{VBE}, respectively. These states would be combined by an interaction Hamiltonian of the form

$$H = \begin{pmatrix} \delta_B & \gamma \\ \gamma & \delta_{VBE} \end{pmatrix}$$

where γ is the coupling constant. The well-known solutions to this problem are $|\Psi_d{}^{\pm}\rangle = a^{\pm}|\phi_B\rangle + b^{\pm}|\psi_{VBE}\rangle$, with one of them being upshifted from the band edge state (the E^+ state; we here assume $\delta_B < \delta_{VBE}$), and the coefficients satisfy the equation

$$a^{\pm} = \frac{\gamma}{(E^{\pm} - \delta_B)} b^{\pm} \tag{4}$$

where the eigenvalues $E^{\pm}$ are given by

$$E^{\pm} = \frac{\delta_{VBE} + \delta_B \pm \sqrt{(\delta_{VBE} - \delta_B)^2 + 4\gamma^2}}{2} \tag{5}$$

In the limit of weak coupling, $\gamma \ll (\delta_{VBE} - \delta_B)$, the split impurity level has energy $E^+ - \delta_{VBE} \approx \gamma^2/(\delta_{VBE} - \delta_B)$, and then we get PDOS/DOS $\approx a^+/b^+ \approx \gamma/(\delta_{VBE} - \delta_B)$. Thus, we see that the PDOS/DOS ratio is proportional to the coupling. When the impurity is on the surface, the coupling to the band edge state is basically via the surface states. In a configuration such as position 4 in NW1 or position 5 in NW2, where the surface states contribute more strongly to the formation of the band edges,[22] the coupling will be stronger. The stronger coupling can be associated with deeper impurity levels, and indeed the data in Table 4 confirm this trend. A large weight of the dopant atom at the impurity levels means that the extra electron or hole is more tightly bound to the dopant and thus less spread through the system. Thus, unlike what happens for impurities adsorbed on the facets of the wires, substitutional dopants located on active facets (in the sense of ref 22) tend to be deeper and thus less effective in changing the systems electric properties.

The trends presented by the data in Table 3 are in very close agreement with Table 4, in particular, the extremely low value for the Mott-Hubbard energy for NW1 doped with

phosphorus on position 3, the canted <001> facet. As observed in Table 4, even for the ultrathin wire NW1, the PDOS/DOS ratio is of the same order as in the P-doped bulk. In ref 22, we showed that the relevance of the canted <001> facet is even lower at the conduction band minimum than for the valence band maximum, which explains why on these surfaces the donor levels are more delocalized than the acceptor levels. This indicates that, in this particular position, doping with phosphorus is more effective than with boron. This situation is reversed for all other sites studied, according to the total energy and the PDOS analyses.

Comparison of the data in Table 4 for NW1, NW3, and the bulk also indicates that, for NWs of diameters starting from around 3 nm, the dopant levels already should have a fairly shallow character. A similar estimate for P-doped Si nanocrystals led to the conclusion that bulk-like impurity states would only be observed at larger systems, with diameters around 20 nm.[25] In that work, it was shown that the more confined the nanocrystals are, the smaller is the bohr radius and the deeper is the potential well associated with the impurity atom: that is, the extra electron is more tightly bound to the impurity and thus less capable of effectively doping the system. Our results confirm this trend. Nevertheless, as NWs are less confined than quantum dots, it is expected that the bulk doping regime will be achieved at smaller dimensions, as our results indicate. Finally, in ref 32, a semiempirical tight-binding Hamiltonian analysis led to the conclusion that impurity levels in Si NWs of diameters as large as 20 nm would still display a deeper character than in the doped Si bulk. Such diameter for bulk-like doping to be recovered seems unexpectedly high, especially if compared with the predictions of ref 25 for Si NCs, as discussed above. The discrepancy between the results of ref 22 and our results might be related to the difficulty in correctly parametrizing the tight-binding Hamiltonian for wires, which as we have seen, are extremely sensitive to slight structural variations, such as lattice parameter and type of faceting. Nevertheless, the general trend about how the character of the impurity levels evolve according to the confinement is similar to our results.

In summary, we conclude that, unlike alleged in previous works, B impurities in Si NWs will be rather uniformly distributed within the wires and on their surfaces, given that the differences in the formation energies of defects on different substitutional sites tend to decrease as the diameter of the wires approach realistic dimensions (more than 30 Å). For P-doped wires, the differences in formation energies among different sites decrease more slowly than in B-doped ones, but the trend remains similar. Impurity states will present different electronic behavior on different surfaces and the more confined the system is, the deeper the impurity levels will be. Finally, for NWs of realistic diameters, the dopant induced levels will have a shallow character.

Acknowledgment. The authors acknowledge C. G. Van de Walle, J. Neugebauer, and M. P. Lima for useful discussions. We also acknowledge Brazilian agencies FAPESP and CNPq for financial support and CENAPAD-SP for computational time.

References

(1) Law, M.; Goldberger, J.; Yang, P. D. *Ann. Rev. Mater. Res.* **2004**, *34*, 83.
(2) (a) Lu, W.; Lieber, C. M. J.; Phys, D. *Appl. Phys.* **2006**, *39*, R387. (b) Wu, Y.; Cui, Y.; Huynh, L.; Barrelet, C. J.; Bell, C. D.; Lieber, C. M. *Nano Lett.* **2004**, *4*, 433.
(3) Cui, Y.; Zhong, Z.; Wang, D.; Wang, W.; Lieber, C. M. *Nano Lett.* **2003**, *3*, 149.
(4) Duan, X.; Niu, C.; Sahi, V.; Chen, J.; Parce, J. W.; Empedocles, S.; Goldman, J. L. *Nature* **2003**, *425*, 274.
(5) Cui, Y.; Lieber, C. M. *Science* **2001**, *291*, 851.
(6) Schmidt, V.; Senz, S.; Gösele, U. *Nano Lett.* **2005**, *5*, 433.
(7) Cui, Y.; Duan, X.; Hu, J.; Lieber, C. M. *J. Phys. Chem. B* **2000**, *22*, 5213.
(8) Ma, D. D.; Lee, C. S.; Lee, S. T. *Appl. Phys. Lett.* **2001**, *79*, 2468.
(9) Fukata, N.; Chen, J.; Sekiguchi, T.; Okada, N; Murakami, K.; Tsurui, T.; Ito, S. *Appl. Phys. Lett.* **2006**, *89*, 203109.
(10) Fukata, N.; Chen, J.; Sekiguchi, T.; Matsushita, S.; Oshima, T.; Uchida, N; Murakami, K.; Tsurui, T.; Ito, S. *Appl. Phys. Lett.* **2007**, *90*, 153117.
(11) Whang, S. J.; Lee, S.; Chi, D. Z.; Yang, W. F.; Cho, B. J.; Liew, Y. F.; Kwong, D. L. *Nanotechnology* **2007**, *18*, 275302.
(12) (a) Fernández-Serra, M. V.; Adessi, C.; Blase, X. *Phys. Rev. Lett.* **2006**, *96*, 166805. (b) Fernández-Serra, M. V.; Adessi, C.; Blase, X. *Nano Lett.* **2006**, *6*, 2674.
(13) Peelaers, H.; Partoens, B.; Peeters, F. *Nano Lett.* **2006**, *6*, 2781.
(14) Markussen, T.; Rurali, R.; Jauho, A. P.; Brandbyge, M. *Phys. Rev. Lett.* **2007**, *99*, 76803.
(15) Our results are based on fully ab initio DFT[16] calculations. The exchange-correlation potential was treated through GGA-PBE flavor.[17] The core potentials were represented by nonlocal pseudopotentials,[18] whereas Kohn-Sham orbitals were written in terms of DZP basis set[19] (SIESTA code).[20] For the Brillouin zone sampling, a (1 × 1 × 5) set was used, where the *z* direction is along the wires' axes. All of the structures were fully optimized using the CG algorithm with convergence criterium of 0.025 eV/Å. The supercell method with periodic boundary conditions was adopted. NW1, NW2, and NW3 have supercells of 4 planes along the growth direction, with 80, 88, and 216 atoms, respectively. NW1-b possesses 7 atomic planes along the growth direction (200 atoms). The lateral sides of the supercells were enough to prevent interaction between NWs and their images for neutral states. A cutoff of 200 Ry for the grid integration was utilized to represent the charge density.
(16) (a) Hohenberg, P.; Kohn, W. *Phys. Rev.* **1964**, *136*, 864B. (b) Kohn, W.; Sham, L. J. *Phys. Rev.* **1965**, *140*, 1133A
(17) Perdew, J. P.; Burke, K.; Ernzerhof, M. *Phys. Rev. Lett.* **1996**, *77*, 3865.
(18) Troullier, N.; Martins, J. L. *Phys. Rev. B* **1991**, *43*, 1993.
(19) Sankey, O. F.; Niklewski, D. J. *Phys. Rev. B* **1989**, *40*, 3979.
(20) (a) Ordejón, P.; Artacho, E.; Soler, J. M. *Phys. Rev. B* **1996**, *53*, 10441. (b) Sánchez-Portal, D.; Artacho, E.; Soler, J. M. *Int. J. Quantum Chem.* **1997**, *65*, 453.
(21) Ma, D. D.; Lee, C. S.; Au, F. C.; Tong, S.; Lee, S.T. *Science* **2003**, *299*, 1874.
(22) Leao, C. R.; Fazzio, A.; da Silva, A. J. R. *Nano Lett.* **2007**, *7*, 1172.
(23) Cantele, G; Degoli, E; Luppi, E.; Magri, R.; Ninno, D; Iadonisi, G.; Ossicini, S. *Phys. Rev B* **2005**, *72*, 113303.
(24) Xu, Q.; Luo, J.-W.; Li, S.-S.; Xia, J.-B.; Li, J.; Wei, S.-H. *Phys. Rev B* **2007**, *75*, 235304.
(25) Chan,T.-L. ; Tiago, M. L. ;Kaxiras, E. ; Chelikowsky, J. R., *Nano Lett.* 2007, printed on web.
(26) The bulk ionization level comes as slightly negative (−0.06 eV). This is caused mainly by the large proximity between the B atom in the supercell and its images.
(27) Zhang, S. B.; Northrup, J. E. *Phys. Rev. Lett.* **1991**, *67*, 2339.
(28) Persson, C.; Zhao, Y.-J.; Lany, S.; Zunger, A. *Phys. Rev. B* **2005**, *72*, 035211.
(29) Makov, G.; Payne, M. C. *Phys. Rev. B* **1995**, *51*, 4014.
(30) Analysis for the wires in several different supercells showed that the lowest achievable value for the Hartree potential in the vacuum region occurred when the dimensions of the supercell perpendicular to the wire's axes were about twice the wire's average diameter. This signalizes a minimum for the intercell electrostatic interaction, yielding the most accurate values for the Mott-Hubbard energy and charge level crossings in Table 3.
(31) Kagimura, Nunes, R.; Chacham, H. *Phys. Rev. Lett.* 2006.
(32) Diarra, M.; Niquet, Y.-M.; Delerue, C.; Allan, G. *Phys. Rev. B* **2007**, *40*, 45301.

NL080403D